Stability and Spectral Behavior of Grating-Controlled Actively Mode-Locked Lasers

Arthur James Lowery, Noriaki Onodera, *Member, IEEE,* and Rodney S. Tucker, *Fellow, IEEE*

Abstract—**Amplitude, timing, and wavelength instabilities in a semiconductor mode-locked laser are studied experimentally and by using an accurate numerical model. It is shown that these instabilities can occur when the RF drive frequency is tuned to give a minimum average pulsewidth. We show that experimental measurement techniques, such as sampling and averaging, can mask these instabilities. Using our numerical model, we show that the wavelength instability is associated with the amplitude and timing instabilities and that the large broadening of the optical spectrum observed experimentally is caused by a cyclic wavelength instability.**

I. Introduction

ACTIVELY mode-locked lasers are attractive as sources of periodic trains of short optical pulses. Applications of mode-locked pulses include very-high bit-rate communications [1], instrumentation [2], and optical computing [3]. Much progress towards short pulses has been made in recent years, with pulsewidths down to fractions of a picosecond being reported [4]. A limit to performance of systems employing short optical pulses is amplitude, timing, and wavelength instability of the pulses. Timing and spectral instabilities could result in intersymbol interference and degraded receiver sensitivities in communications systems, accuracy limitations in instrumentation, and errors in optical computers.

Measurements of the detected RF spectrum [5], [6] have shown line broadening which has been attributed to noise-induced instabilities in the amplitude and phase (timing) of the pulses. However, a low jitter level was shown [6] to be critically dependent on the operating conditions of the laser, in particular, the detuning (or offset) of the RF drive frequency from the external cavity fundamental resonance frequency. Numerical simulations of actively mode-locked lasers have shown large *cyclic* variations in pulse amplitude and timing can occur when the RF frequency is increased by a few MHz from the frequency for minimum pulsewidth [7]–[11].

Little has been reported on experimental measurements of the spectral behavior of mode-locked lasers as a function of detuning. Lowery and Marshall have studied the optical spectrum from a mode-locked laser using numerical simulations and showed the effects on the spectrum of the linewidth enhancement factor, ac drive current, dc bias current, imperfect antireflection coating on one of the laser facets, and of driving at a harmonic of the cavity resonance frequency [10].

The objective of this paper is to assess the amplitude, timing, and spectral stability of mode-locked lasers with dispersive gratings over a wide range of detunings. It is shown that the instabilities can occur when the laser is adjusted for a minimum average pulsewidth. We compare experimental measurements with numerical simulation results from the transmission-line laser model (TLLM) [8]–[12]. The numerical simulations include models of the measuring equipment. This modeling of the measurement equipment involves: 1) averaging many pulses together to obtain an average pulse shape, 2) overlaying samples from many pulses to simulate a nonaveraging sampling oscilloscope, and 3) averaging the spectrum of many pulses to simulate the operation of a monochromator. Excellent agreement between the experimental measurements and the processed numerical simulation results are demonstrated.

The numerical model is able to simulate a time sequence of pulses that would be difficult to measure experimentally. The model can readily simulate instabilities in the pulsewidth, pulse amplitude, and pulse timing. The model shows that these instabilities are cyclic rather than random and appear experimentally as an apparent broadening of the sampling oscilloscope traces. This cyclic behavior is confirmed by side bands in the measured RF spectrum of the detected pulses. In addition, the model shows cyclic instabilities in the wavelength of the numerically generated pulses. These wavelength instabilities are related to the cyclic instabilities in the time domain. These wavelength instabilities are difficult to measure experimentally, but can cause a large spectral broadening of the average spectrum, as seen experimentally using a monochromator.

Section II of this paper describes the mode-locked laser together with the measurement apparatus. Section III describes the numerical model and additional post-processing algorithms. Section IV presents the experimental results together with the numerical results and shows the effect of detuning on average pulsewidth, pulse stability,

Manuscript received January 7, 1991; revised May 20, 1991. This work was supported by the Australian Research Council by Grant A49030281 and the Australian Telecommunications and Electronics Research Board.

The authors are with the Photonics Research Laboratory, Department of Electrical and Electronic Engineering, University of Melbourne, Parkville, Victoria 3052, Australia.

IEEE Log Number 9103212.

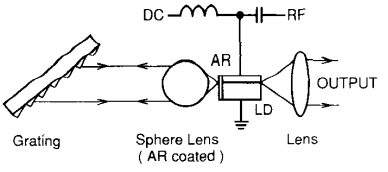

Fig. 1. Mode-locked laser. LD is the laser diode chip and AR is the antireflection-coated facet.

and optical spectrum; the discussion and conclusions are presented in Section V.

II. Experimental Arrangement

The mode-locked laser under study is shown in Fig. 1. It comprises a 1500 nm laser with an antireflection-coated (better than 0.1% reflectivity) rear facet coupled to an external cavity using a 2 mm diameter antireflection coated sphere lens. The external cavity mirror is formed with a 1200 lines/mm diffraction grating with a blaze wavelength of 750 nm. This grating controls the lasing wavelength and system bandwidth. The grating bandwidth is estimated to be approximately 100 GHz, based on a measurement of the spot size on the grating.

The RF drive to the laser is superimposed on a constant dc bias using a commercial bias tee. The drive signal is supplied by a Hewlett-Packard synthesized signal generator (8341B) with a Mini-Circuits amplifier (ZHL-42) to boost the power. The drive frequencies are around 2 GHz at power levels up to 30 dBm.

The parameters for the experimental system and those used in the numerical model are summarized in Table I. Coupling between the laser and the grating was optimized by adjusting for minimum threshold current. Similarly, the grating angle was adjusted to minimize the threshold current, thereby ensuring that the device was operated close to the gain peak wavelength. This is not necessarily the wavelength for minimum pulsewidth, because higher differential gains are possible at shorter wavelengths [10]. The laser was adjusted to produce the shortest pulses possible (as measured on the sampling oscilloscope) by adjusting the RF drive power to around 28 dBm and selecting a dc bias level around 129% of threshold.

Three instruments were used to measure the performance and stability of the laser. The pulse shape was monitored using a Tektronix sampling oscilloscope (CSA 803) with a SD-26 sampling head (risetime <18 ps) closely coupled to a high-speed p–i–n photodetector (risetime <12 ps). The optical spectrum was measured using an Anritsu optical spectrum analyzer (MS9001A1) with a measured resolution of 0.75 nm at 1500 nm. The RF spectrum of the detected pulses was measured with a Hewlett-Packard optical signal analyzer (HP70000).

III. Numerical Model

Many analytical and numerical models have been developed for mode-locked lasers. Analytical models commonly assume stable pulses in order to develop an analytical expression for pulsewidth and cannot be used to predict instability. This is sometimes known as the "self-reproducing profile" (SRP) approach [13]–[16]. In contrast, numerical models can, in general, simulate instabilities.

TABLE I
Laser Parameters

Symbol	Parameter Name	Value	Unit
λ	Grating Wavelength	1.50	μm
L	Laser Chip Length	300.0	μm
w	Active Region Width	2.0	μm
d	Active Region Depth	0.15	μm
L_e	External Cavity Length	76.68	mm
Δf	Grating Bandwidth	100.0	GHz
N_0	Transparency Carrier Density	1.0×10^{18}	cm^{-3}
a	Gain Cross Section	3.5×10^{-16}	cm^2
Γ	Waveguide Confinement Factor	0.35	
α	Linewidth Enhancement Factor	5.6	
n_e	Group Index of Waveguide	4.0	
α_w	Waveguide Attenuation Factor	30.0	cm^{-1}
R_f	Front Facet Reflectivity	30.0	%
R_r	Rear Facet Reflectivity	0.1	%
R_e	External Cavity Coupling	2.9	%
A	Monomolecular Recomb. Coef.	1.0×10^{8}	s^{-1}
B	Bimolecular Recomb. Coef.	8.6×10^{-11}	$cm^3 \cdot s^{-1}$
C	Auger Recomb. Coef.	4.0×10^{-29}	$cm^6 \cdot s^{-1}$
β	Spontaneous coupling per laser chip mode	4.0×10^{-5}	

Demokan [17] developed a time-domain numerical model, based on photon-density rate equations, which was able to show the growth of mode-locked pulses after the laser was turned on. However, long term instabilities, after the turn on transient, were not reported. Recently, Demokan's model was extended by Morton *et al.* [7] to predict cyclic instabilities in mode-locked lasers optimized to produce subpicosecond pulses. Morton's studies neglected dispersion within the laser cavity. This assumption is unrealistic because it requires, for stable pulses, that the round-trip gain is unity for all points on the pulse. In reality, this condition of unity round-trip gain will be relaxed because of pulse spreading due to dispersive elements within the resonant cavity. The relaxation of the unity round-trip gain condition, because of pulse spreading, means that the laser can maintain pulse stability over a greater range of operating conditions.

Models based on solution of traveling-wave equations for optical field rather than photon density can include dispersive elements such as gratings. One such model is the transmission-line laser model (TLLM) which was applied to the modeling of mode-locked lasers by Lowery [8]. Results from the TLLM show instabilities in mode-locked lasers for certain detunings [8], [9], [11]. In other simulations of mode-locked lasers using the TLLM, good agreement with experimental results have been obtained [10], [18]. A model similar to the TLLM has been developed by Werner and Lee [19] who showed that pulse energy jitter was a function of bias current. A similar result has been obtained using the TLLM [8]. The transmission-line laser model will be used in this paper.

A. The Transmission-Line Laser Model

The TLLM is based on a transmission-line analog of the optical cavity inside and outside the laser chip. This analog allows the wave equations within the cavity to be solved efficiently using a computer. Thus, all the optical resonances of the cavity may be found. A detailed description of the TLLM is given in [12]. The laser is divided longitudinally into sections and transmission lines represent the axial propagation delays of the optical waves through each section. Scattering matrices represent optical gain, phase shift, attenuation, and spontaneous noise within each section. The transmission-line analog is solved iteratively in the time domain, with the iteration timestep equal to the propagation delay between equally spaced scattering matrices.

The advantages of using such a model are that it can include many details and parameters. For example, it includes information about optical field, rather than photon density. Thus, cavity resonances can be included in the model over a wide spectral bandwidth [12]. The optical spectrum can be found by a simple Fourier transform of the output field. This allows the spectral stability of lasers to be determined. The model also includes a dependence of the refractive index on carrier concentration which gives rise to self-phase modulation and hence wavelength shifting of the light [20].

The model is similar to earlier transmission-line laser models for mode locking [8]–[11], [18]. However, two modifications have been made to enhance the accuracy of the model.

Modification One: Helkey *et al.* [21] have improved the accuracy of the photon-density model by using partial integration within each model section. Partial integration assumes the photon density within each model section grows exponentially across that section. The average photon density within that section can then be calculated from the incoming photon density assuming this exponential growth. The average photon density is then used to calculate the stimulated emission rate. Previous TLLM's assumed that the average photon density was approximately the input photon density, so underestimated the stimulated emission rate. The TLLM now calculates the average photon density using Helkey's method producing a small improvement in the accuracy of the output power.

Modification Two: In previous TLLM's of mode-locked lasers the changes in refractive index inside the laser chip were calculated from the average carrier density within the chip. This approximation is strictly not correct for optical pulses shorter than the transit time of the chip because the pulse is only affected by the refractive index of the material while it is passing through, and not the average index of the whole chip. To correct this approximation, the TLLM now calculates the refractive index within each model section from the carrier density within that section [22]. This modification has little effect on the spectral results from the model.

In common with other numerical mode-locked laser models, the following assumptions are made:

1) single lateral/transverse mode operation,
2) homogeneous current injection (though not a requirement)
3) a dispersionless laser medium.

All of the above are realistic assumptions for lasers with pulsewidths greater than a picosecond and dispersion dominated by an external grating.

In all the simulations described here, a five-section model was used to represent the laser chip. This gave a timestep of 0.8 ps and a modeled optical bandwidth of 6.25 THz. The grating was modeled with a Lorentzian response with a FWHM of 100 GHz. The gain spectrum of the active material was assumed to be flat because the grating was assumed to be the dominant bandwidth-limiting mechanism. The model was reinitialized for each simulation and was allowed to run for 40 000 iterations which allowed any initial transient stabilities to settle. Reinitialization is equivalent to turning the laser off, then on, before each measurement and ensures independence of the simulation results. However, random number noise generators representing spontaneous emission followed the same sequence for each run so that the differences in the results cannot be attributed to random noise alone.

B. Post Processing Algorithms

The output of the TLLM is a sampled version of the optical field. This can be squared and smoothed over one optical cycle to give the intensity of the field as a function of time. The intensity waveform contains all instabilities in the output of the laser. However, because of sensitivity and data capture limitations, most high-speed experimental measurements rely on some sort of averaging over many pulses to achieve a high bandwidth and sensitivity. To allow comparison between the modeled results and those obtained experimentally, two post-processing algorithms were developed.

Algorithm One: This algorithm uses box-car averaging of many pulses to obtain an average pulse shape as would be seen with a digital oscilloscope in averaging mode or on a synchroscan streak camera. Obviously, pulses averaged in this manner appear perfectly stable even when the unaveraged intensity waveforms show large amplitude, width and timing jitters. This point will be illustrated in Section IV-A.

Algorithm Two: This algorithm overlays samples from sequential pulses in a manner similar to a digital sampling oscilloscope with a very long persistence and without signal averaging. Pulse instability shows as a broadening of the trace, because pulses will not lie on top of one another. This algorithm is used to compare experimental and simulated pulse stability in Section IV-B.

Optical spectra can be also obtained from the model by Fourier transformation of the optical field samples. If the transform is taken over several pulses, then the external cavity modes can be resolved. A transform taken over several pulses also produces the average spectrum of these pulses, as would be obtained with most scanning monochromators and interferometers. To allow comparison

with our monochromator, which could not resolve the individual modes, we convolved the modeled spectrum with a Gaussian function with a FWHM of 0.75 nm. Comparisons between simulated and measured spectra are presented in Section IV-E.

IV. Results

A. Averaged Pulsewidth Versus Detuning

Fig. 2 shows the measured and simulated average pulsewidth versus detuning. The simulated pulsewidth was obtained using algorithm one, as described in Section III-B. The cavity resonance frequency, hence the absolute detuning, is difficult to measure experimentally. Thus, we labeled zero detuning as that for the shortest stable pulses. The two curves are in good agreement for all detunings. The difference in pulsewidth for short pulsewidths can be explained by the risetime of the experimental measurement system, which was not included in the numerical simulations. The curves are asymmetrical, there being a rapid decrease in pulsewidth as the detuning is increased, followed by a slow increase in pulsewidth. This asymmetry is in broad agreement with the experimental measurements of Chen *et al.* [23], van der Ziel [13], and Kempf and Garside [15]. The regions of instability and stability are marked on Fig. 2. These were determined by examination of sequences of pulses generated numerically. The unstable pulses have large, cyclic variations in amplitude, width and timing, and are detailed below.

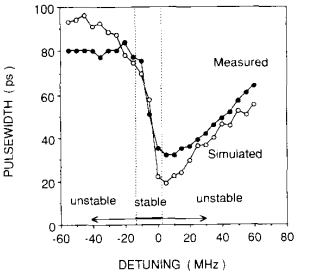

Fig. 2. Average pulsewidth versus detuning: ● measured, ○ simulated.

B. Pulse Stability Versus Detuning

The digital sampling oscilloscope can be used to assess pulse stability when set to infinite persistence mode. In this mode, every sample point is displayed so that a plot of all possible pulse shapes is gradually built up. If there is pulse instability, the samples will be scattered, forming a broad trace. We recorded the oscilloscope traces at detunings of −30, −10, 0, and +30 MHz, as shown in Fig. 3(a)–(d), respectively. The RF drive waveform to the laser was also monitored with the sampling oscilloscope to ensure that the observed instabilities were not a result of unreliable oscilloscope triggering. At a detuning of −30 MHz [Fig. 3(a)], instabilities occurred on the trailing edge of the pulse and the pulse was broad. At −10 MHz [Fig. 3(b)], the pulse became very stable, but broad (70 ps) and asymmetrical, with a slow trailing edge. At 0 MHz, the detuning for the shortest pulse [Fig. 3(c)], the pulse had two distinct peaks, the first being 32 ps wide. The peaks were both symmetrical and the pulses were stable. The amplitude of the secondary peak increased with higher dc bias currents and the pulses became unstable if the detuning was increased beyond this point. At +30 MHz [Fig. 3(d)], the pulse was single peaked, but suffered from large instabilities, these instabilities being at the center of the pulse.

We simulated the infinite persistence results, above, using the TLLM and algorithm two as described in Section III-B. These are shown in Fig. 3(e)–(h) which correspond to the experimental results in Fig. 3(a)–(d), respectively. The simulations showed the same trends as the experimental results above. However, much greater instabilities were observed at the detunings of −30 and +30 MHz [Fig. 3(e) and (h)]. Careful examination of Fig. 3(e) shows that the instability is greatest on the trailing edge

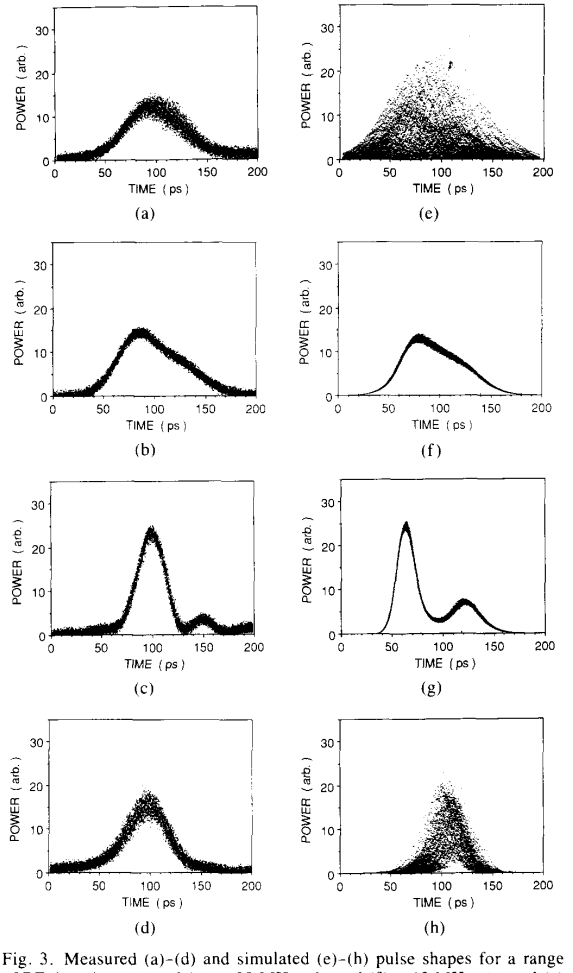

Fig. 3. Measured (a)–(d) and simulated (e)–(h) pulse shapes for a range of RF detunings (a) and (e): −30 MHz; (b) and (f) −10 MHz; (c) and (g) 0 MHz; (d) and (h) 30 MHz.

of the pulse, as observed experimentally in Fig. 3(a). Similarly, Fig. 3(h) shows greatest instability at its center, as observed in Fig. 3(d). Note that some of these instabilities may be smoothed in experimentally by the finite bandwidth of the photodetector and the sampling head, in particular, pulses with closely spaced double peaks may be displayed as single peaked pulses. At detunings of -10 and 0 MHz [Fig. 3(f) and (g)], excellent agreement was obtained between theory and experiment. Only small instabilities were seen in the pulses; these were probably masked by instrumentation noise in the experiment.

A simulated single-shot sequence of ten pulses, corresponding to the detuning of Fig. 3(d) and (h) ($+30$ MHz), is shown in Fig. 4. This Figure shows the large pulse-to-pulse variations in pulse shape and amplitude that cause the large scatter of samples in Fig. 3(h). The explanation of these instabilities is as follows. Because the RF drive frequency is considerably larger than the cavity resonance frequency, the gain within the laser chip peaks well before the return of the optical pulse from the external cavity. This means that the growth of a new pulse, preceding the returning pulse, is favored by the chip gain (pulses marked *A–E*, Fig. 4). The new pulse grows to dominance because it receives more gain per round-trip than the old pulse (pulses marked *F–I*). This process repeats: pulses *G–J* have a new pulse preceding them as did pulses *A–E*. A similar process, but where the optical pulse returns from the optical cavity early, explains the instabilities measured at a detuning of -30 MHz [Fig. 3(a) and (e)].

To confirm the cyclic nature of the amplitude and timing instabilities, we measured the RF spectrum of the pulse train. The spectra for all detunings are shown in Fig. 5(a)–(d). For detunings of -30 and $+30$ MHz [Fig. 5(a) and (d)] the spectrum showed broad side bands spaced at approximately 120 MHz from the RF drive frequency. These side bands confirm the cyclic nature of the instabilities: noise-induced instabilities would simply broaden the 2 GHz spectral peak [6]. The $+30$ MHz detuning spectrum [Fig. 5(d)] showed multiple side bands which may indicate phase modulation of the pulses arising from cyclic timing instabilities. The -10 MHz detuning [Fig. 5(c)] spectrum showed least broadening of the 2 GHz resonance, indicating that tuning for wider pulses improves overall stability.

C. Optical Spectral Width Versus Detuning

The measured spectral width and the simulated spectral width, averaged over many pulses in both cases, are plotted for a range of detunings in Fig. 6. The experimental and numerical results are in good agreement and the spectral width increases more than fourfold when the pulses become unstable for positive detunings. A smaller increase in spectral width occurs as the pulses become unstable for negative detunings. In the stable regime, the spectral widths are approximately 0.1 nm (13 GHz).

A common measure of the performance of a mode-locked laser is the time–bandwidth product (TBP). When

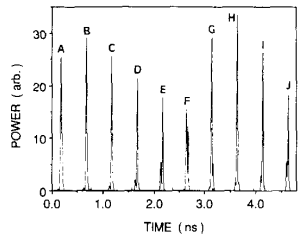

Fig. 4. Single-shot simulated output corresponding to Fig. 3(d) showing instabilities in the pulse shape, amplitude, and timing.

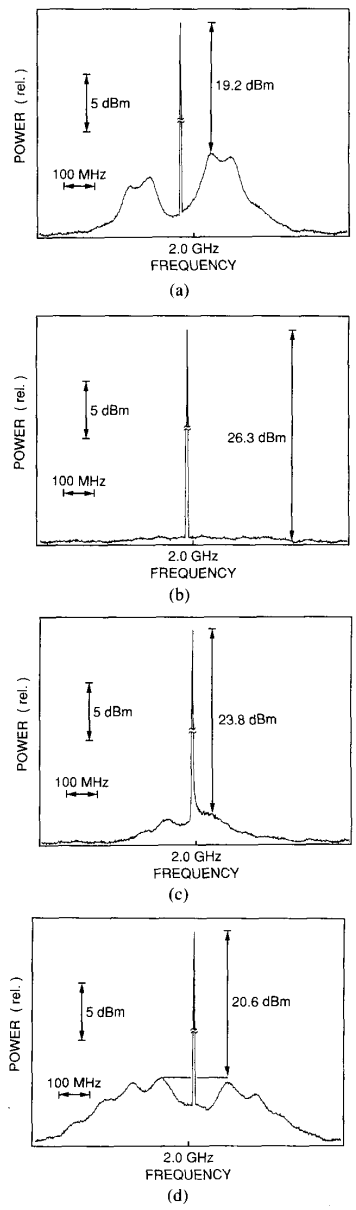

Fig. 5. Measured RF spectrum of detected pulses for a range of RF detunings. (a) -30 MHz; (b) -10 MHz; (c) 0 MHz; (d) 30 MHz.

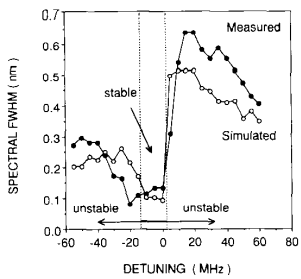

Fig. 6. Average spectral width of pulses versus RF drive frequency: ● measured, ○ simulated.

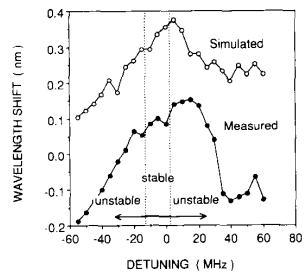

Fig. 7. Center wavelength of the optical spectra versus RF drive frequency: ● measured, ○ simulated.

the TBP is close to the value expected for a particular pulse shape, the pulses are said to be transform limited. Experimentally measured TBP's in the range 0.3 to 0.6 have been reported [8]. For comparison, unchirped Gaussian pulses have theoretical TBP's of 0.441 and sech^2 pulses have theoretical TBP's of 0.315. We calculated the numerical and the measured TBP's for the zero detuning case of our laser. The experimentally measured TBP was 0.587 and the numerically simulated TBP was 0.254. This discrepancy is partially due to the measured pulsewidth being increased by the risetime of the measuring instruments. However, the TBP increased substantially in the unstable regimes of the detuning curve. For +30 MHz detuning, the TBP was 2.87 experimentally, and 2.00 numerically. For −30 MHz detuning the TBP was 1.73 experimentally and 2.44 numerically. The pulse shapes for these detunings were nearly Gaussian, suggesting that the TBP should be close to 0.441.

D. Optical Wavelength Versus Detuning

The measured and simulated center wavelengths of the averaged spectra are plotted in Fig. 7. The experimental and simulated results show the same trend of increasing red shift as the detuning is increased for detunings up to 5 MHz; further increases in detuning cause the wavelength to decrease. There is a constant offset between the experimental and simulated curves. This may be caused by experimental error; the center wavelength of the grating was measured by monitoring the below-threshold CW spontaneous emission spectrum and may have drifted during the experiment.

The shift in the peak of the spectrum towards red and away from the grating peak wavelength can be explained by self-phase modulation of the pulse as it passes through the laser chip [20]. The amount red shift of the spectral peak is proportional to the rate of carrier depletion. At low RF drive frequencies, the optical pulse returns from the external cavity while the RF component of the injection current is still flowing into the active region. Thus, carrier depletion by stimulated emission is opposed by carrier injection, therefore little red shift occurs. Also, because the carrier concentration has not built up to its maximum value before the return of the optical pulse, the optical gain, hence carrier depletion by stimulated emission, is low. If the RF frequency is increased, the optical pulse returns when the RF component of injection current is approaching zero. Thus, the carrier depletion by stimulated emission is not opposed by this current. Also, the carrier concentration builds up to higher levels before the return of the optical pulses and the stimulated emission rate is increased. For these two reasons more red shift occurs at higher detunings.

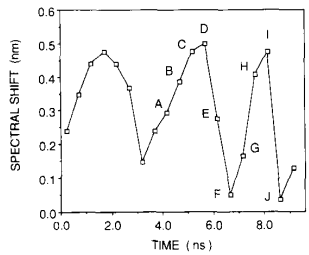

Fig. 8. Optical wavelengths of simulated pulses for a detuning of +30 MHz showing a cyclic wavelength jitter. Labels correspond to those in Fig. 4.

At very high positive detunings, the pulse is unstable in position with respect to the gain waveform, as shown in Fig. 3(d) and (h) and Fig. 4. Because the wavelength shift due to SPM is dependent on the pulse position with respect to the RF drive, the pulses arriving back at the laser chip late will be red shifted and the early pulses will be unshifted. Fourier transformation of numerical data corresponding to each pulse in Fig. 4 showed that the wavelength of the pulses varied cyclically. The wavelengths of the individual pulses shown in Fig. 4 are plotted in Fig. 8. Comparison of Figs. 4 and 8 show that pulses returning from the external cavity late, with respect to the chip gain waveform peak, experience a large red shift in wavelength; new pulses, which arrive early, experience little wavelength shift. When the individual pulses' spectra are averaged, a broad spectrum results. This wavelength jitter explains the large time-bandwidth product which would not be expected if the pulses were stable and Gaussian. At large negative detunings much less spectral broadening in the unstable region occurs because the injection current always opposes the carrier depletion.

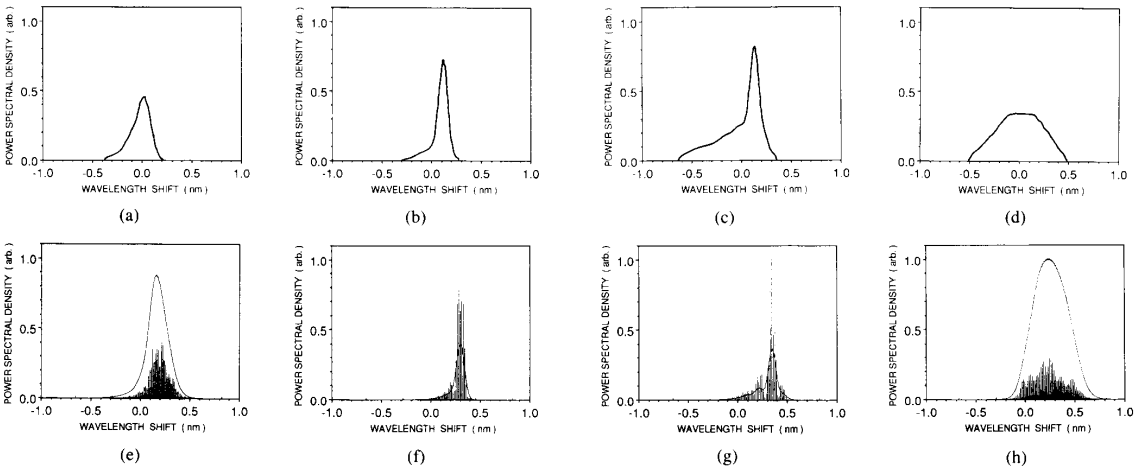

Fig. 9. Measured (a)-(d) and simulated (e)-(h) optical spectra for a range of RF detunings (a) and (e): −30 MHz; (b) and (f) −10 MHz; (c) and (g) 0 MHz; (d) and (h) 30 MHz.

TABLE II
EFFECTS OF DETUNING

Measurement	Detuning (MHz)			
	−30	−10	+0	+30
Ave. Pulsewidth (Fig. 2)	Large	Large	Minimum	Medium
Pulse Shape (Fig. 3)	Symmetrical	Slow Tail	Second Pulse	Symmetrical
Pulse Stability (Figs. 3 and 4)	Unstable	Stable	Stable	Unstable
RF Spectrum (Fig. 5)	Strong Sidebands	No Sidebands	Weak Sidebands	Multiple Sidebands
Spectral Width (Fig. 6)	Medium	Small	Small	Large
Peak Wavelength (Fig. 7)	Blue shifted	Red shifted	Red shifted	Unshifted
Wavelength Stability (Fig. 8)	Unstable	Stable	Stable	Unstable
Optical Spectrum (Fig. 9)	Nearly Symmetrical	Blue Tail	Blue Tail	Symmetrical
TBP (experimental)	1.73	1.07	0.59	2.87
TBP (numerical)	2.44	0.90	0.25	2.00

E. Average Optical Spectrum Versus Detuning

Fig. 9(a)-(d) shows the variation in measured optical spectrum for four different detunings of −30, −10, 0, and 30 MHz. Note that the monochromator averages the spectrum over many pulses. These spectra correspond, respectively, to the pulses shown in Fig. 3(a)-(d) and Fig. 3(e)-(h). At −30 MHz detuning [Fig. 9(a)] the spectrum is almost symmetrical with little wavelength shift. At −10 MHz detuning [Fig. 9(b)] the spectrum narrows and has a red shifted peak. The red shift is caused by SPM, as detailed above. There is also some energy to the blue side of the spectral peak. Time-resolved spectra, obtained using numerical simulations, have shown that the wavelength of a mode-locked laser pulse shifts towards blue after the peak of the pulse [24]. Thus the blue-shifted "tail" of the spectrum observed here corresponds to the slow trailing edge of the pulse shown in Fig. 3(b). The red shift is larger for 0 MHz detuning [Fig. 9(c)] and the blue tail also contains more energy than in Fig. 9(b). The large blue shifted tail corresponds to the secondary pulse as shown in Fig. 3(c). At 30 MHz the spectrum broadens substantially because of the cyclic variation in wavelength. The 30 MHz detuning spectrum appears Gaussian in shape but is far from transform limited, as was shown in Section IV-B.

Fig. 9(e)-(g) shows simulated spectra for the same detunings as in Fig. 9(a)-(d). The simulated plots include both unsmoothed and smoothed results. The unsmoothed results show the external cavity modes of the laser, which are spaced at about 2 GHz. The smoothed simulations allow for comparison with the measured results. The shapes of the measured and smoothed simulated spectra were in

excellent agreement for all detunings. This agreement suggests that the numerical model is well suited to the modeling of mode-locked lasers.

V. Discussion and Conclusion

We have shown that small variations in RF drive frequency affect the stability and performance of grating-controlled mode-locked lasers. The effects of detuning on pulsewidth, pulse stability, and optical spectrum are summarized in Table II. One important result is that when the RF drive frequency is adjusted to give the shortest average pulsewidth, the pulses are unstable. The standard detuning curve (Fig. 2) does not show this, but implies that short pulses may be obtained over a wide range of detunings where there are instabilities. An important conclusion of the present work is that averaged temporal measurements, be they from sampling oscilloscopes, streak cameras, or auto-correlators, must be treated with caution.

We have measured and simulated spectral broadening caused by self-phase modulation within the laser chip. The shortest pulses have red shifted spectra, but also have a blue shifted tail which may be associated with the smaller secondary pulse. Thie tail could possibly be filtered out in practical systems. Unstable pulses have very broad spectra which are far from transform limited. This large increase in the time–bandwidth product is caused by cyclic wavelength variations induced by the timing variations of the optical pulses causing varying amounts of self-phase modulation. These wavelength variations only occur if the pulse is unstable in the time domain. Thus, monitoring of the optical spectrum provides a good indication of the stability of the laser.

Acknowledgment

We wish to achnowledge technical support provided by P. Lee. The laser chip was supplied by G. Raybon of AT&T Bell Laboratories.

References

[1] R. S. Tucker, G. Eisenstein, and S. K. Korotky, "Optical time-division multiplexing for very high bit-rate transmission," *J. Lightwave Technol.*, vol. 6, pp. 1737–1749, 1988.

[2] *Measurement of High-Speed Signals in Optoelectronic Devices: Semiconductors and Semimetals*, vol. 28, R. B. Marcus, Ed. San Diego, CA: Academic, 1990, ch. 5; also "Direct optical probing of integrated circuits and high-speed devices," J. M. Weisenfeld and R. K. Jain.

[3] P. A. Morton, R. J. Helkey, A. Mar, D. J. Derickson, and J. E. Bowers, "Monolithic mode locked laser arrays in optical computing," presented at *SPIE Conf. Opt. Computing*, 1990.

[4] J. E. Bowers, P. A. Morton, A. Mar, and S. W. Corzine, "Actively mode locked semiconductor laser," *IEEE J. Quantum Electron.*, vol. 25, pp. 1426–1439, 1989.

[5] A. J. Taylor, J. M. Weisenfeld, G. Eisenstein, and R. S. Tucker, "Timing jitter in mode-locked and gain-switched InGaAsP lasers," *Appl. Phys. Lett.*, vol. 49, pp. 681–693, 1986.

[6] D. J. Derickson, A. Mar, and J. E. Bowers, "Relative and absolute timing jitter in actively mode-locked semiconductor laser," presented at *12th IEEE Int. Semiconduc. Laser Conf.*, Davos, 1990, paper 17.

[7] P. A. Morton, R. J. Helkey, and J. E. Bowers, "Dynamic detuning in actively mode-locked semiconductor laser," *IEEE J. Quantum Electron.*, vol. 25, pp. 2621–2633, 1989.

[8] A. J. Lowery, "New time-domain model for active mode-locking, based on the transmission-line laser model," *IEE Proc. J: Optoelectron.*, vol. 136, pp. 264–272, 1989.

[9] —"An integrated mode-locked laser design with a distributed-Bragg reflector," *IEE Proc. J.: Optoelectron.*, vol. 138, pp. 39–46, 1991.

[10] A. J. Lowery and I. W. Marshall, "Numerical simulations of 1.5 μm actively mode-locked semiconductor lasers including dispersive elements and chirp," *IEEE J. Quantum Electron.*, vol. 27, pp. 1981–1989, Aug. 1991.

[11] N. Onodera, A. J. Lowery, and R. S. Tucker, "Cyclic wavelength jitter in actively mode-locked semiconductor lasers," *Electron. Lett.*, vol. 26, pp. 220–221, 1991.

[12] A. J. Lowery, "Transmission-line modelling of semiconductor lasers: the transmission-line laser model," *Int. J. Numer. Model.*, vol. 2, pp. 249–265, 1989.

[13] J. P. van der Ziel, "Active mode-locking of double heterostructure lasers in an external cavity," *J. Appl. Phys.*, vol. 52, pp. 4435–4446, 1981.

[14] D. J. Kuizenga and A. E. Siegman, "FM and AM mode-locking of the homogeneous laser-Part 1: Theory," *IEEE J. Quantum Electron.*, vol. 6, pp. 694–708, 1970.

[15] P. Kemph and B. K. Garside, "Dynamics of mode-locked laser diodes employing a repetitive short pulse drive current," *Appl. Opt.*, vol. 26, pp. 4522–4527, 1987.

[16] J. Chen and D. Pan, "A rate-equation analysis of actively mode-locked semiconductor lasers," *IEEE J. Quantum Electron.*, vol. 22, pp. 26–31, 1986.

[17] M. S. Demokan, "A model of a diode laser actively mode-locked by gain modulation," *Int. J. Electron.*, vol. 60, pp. 67–80, 1986.

[18] A. J. Lowery and I. W. Marshall, "Stabilization of mode-locked pulses using a travelling-wave semiconductor laser amplifier," *Electron. Lett.*, vol. 26, pp. 104–106, 1990.

[19] J. Werner and T. P. Lee, "Monte-Carlo simulation of mode-locked semiconductor diode lasers," *Appl. Phys. Lett.*, vol. 57, pp. 1236–1238, 1990.

[20] A. J. Lowery, "Modelling spectral effects of dynamic saturation in semiconductor laser amplifiers using the transmission line laser model," *IEE Proc. J; Optoelectron.*, vol. 136, pp. 320–324, 1989.

[21] R. J. Helkey, P. A. Morton, and J. E. Bowers, "Partial integration method for analysis of mode-locked semiconductor laser," *Opt. Lett.*, vol. 15, pp. 112–114, 1990.

[22] A. J. Lowery, "A new dynamic model for multimode chirp in DFB semiconductor lasers," *IEE Proc.-J: Optoelectron.*, vol. 137, pp. 293–300, 1990.

[23] J. Chen, W. Sibbett, and J. I. Vukusic, "Tunable mode-locked semiconductor lasers incorporating brewster-angled diodes," *Opt. Commun.*, vol. 48, pp. 427–431, 1984.

[24] A. J. Lowery, "Time resolved chirp in mode-locked semiconductor laser," *Electron. Lett.*, vol. 26, pp. 939–940, 1990.

Arthur James Lowery was born in Yorkshire, England, on October 17, 1961. He received the First Class Honours degree in applied physics from Durham University, England, in 1983, and the Ph.D. degree in 1988 from the University of Nottingham.

He then worked as a Systems Engineer at Marconi Radar Systems. In 1984 he was appointed a University Lecturer at the University of Nottingham. In 1990 he became a Senior University Lecturer in the newly-formed Photonics Research Laboratory, University of Melbourne, Australia. He has published more than 40 research papers in the fields of photonics and numerical modeling. His research interests include photonic CAD, mode-locked lasers, laser amplifiers, photonic switching, optical metrology, fiber video distribution, transmission-line modeling, and laser design.

Dr. Lowery is a Chartered Engineer and a member of the Institution of Electrical Engineers.

Noriaki Onodera (M'88) was born in Miyagi prefecture, Japan, on March 13, 1956. He received the B.S., M.S., and Ph.D. degrees in applied physics, all from Tohoku University, Sendai, Japan, in 1979, 1981, and 1985, respectively.

From 1985 to 1990, he was with Ricoh Research Institute of General Electronics, Miyagi, Japan, where he engaged in research on III-V integrated optoelectronic devices for optical signal processing. In 1990, he joined the Photonics Research Laboratory of the University of Melbourne, Australia, as a Research Fellow. His research interests include generation and control of ultrashort pulses from mode-locked semiconductor lasers.

Dr. Onodera is a member of the Institute of Electronics, Information, and Communication Engineers of Japan, the Japan Society of Applied Physics, the American Physical Society, and the IEEE Lasers and Electro-Optics Society,

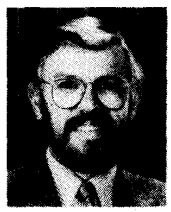

Rodney S. Tucker (S'72-M'75-SM'85-F'90) was born in Melbourne, Australia, in 1948. He received the B.E. and Ph.D. degrees from the University of Melbourne, Australia, in 1969 and 1975, respectively.

From 1973 to 1975 he was a Lecturer of electrical engineering at the University of Melbourne. In 1975 he was awarded a Harkness Fellowship for two years of post-doctoral study in the U.S.A. During 1975-1976 he was with the Department of Electrical Engineering and Computer Sciences, University of California, Berkeley, and during 1976-1977 he was with the School of Electrical Engineering, Cornell University, NY. From 1977 to 1978 he was with Plessey Research (Caswell) Ltd, U.K. and from 1978 to 1983 he was with the Department of Electrical Engineering at the University of Queensland, Brisbane, Australia. From 1984 to 1990 he was with AT&T Bell Laboratories, Crawford Hill Laboratory, Holmdel, NJ. He is currently a Professor of electrical engineering and Head of the Department of Electrical and Electronic Engineering at the University of Melbourne. He is also Director of the Photonics Research Laboratory at the University of Melbourne. His research interests are in the areas of microwave circuits, optoelectronics, and photonic devices and networks. He holds several patents in the area of optoelectronic devices.

Dr. Tucker is a member of the IEEE MTT LIGHTWAVE TECHNOLOGY COMMITTEE and is a member of several international conference technical program committees. He was Editor of the IEEE TRANSACTIONS ON MICROWAVE THEORY AND TECHNIQUES from 1989 to 1990.